

UC Davis

UC Davis Previously Published Works

Title

Modelling the structural response of an eukaryotic cell in the optical stretcher

Permalink

<https://escholarship.org/uc/item/3841p128>

Journal

Current Science, 88(9)

ISSN

0011-3891

Authors

Ananthakrishnan, R
Guck, J
Wottawah, F
[et al.](#)

Publication Date

2005-05-01

Peer reviewed

Modelling the structural response of an eukaryotic cell in the optical stretcher

Revathi Ananthakrishnan^{1,2,3,*}, Jochen Guck^{1,2}, Falk Wottawah^{1,2}, Stefan Schinkinger^{1,2}, Bryan Lincoln^{1,2}, Maren Romeyke¹ and Josef Käs^{1,2}

¹Institute for Soft Matter Physics, University of Leipzig, 04103 Leipzig, Germany

²Center for Nonlinear Dynamics, Department of Physics, University of Texas at Austin, Austin, TX-78712, USA

³Present address: Laboratory for Cell and Computational Biology, University of California at Davis, Davis, CA-95616, USA

The cytoskeleton of an eukaryotic cell is a composite polymer material with unique structural (mechanical) properties. To investigate the role of individual cytoskeletal polymers in the deformation response of a cell to an external force (stress), we created two structural models – a thick shell model for the actin cortex, and a three-layered model for the whole cell. These structural models for a cell are based on data obtained by deforming suspended cells, where each cell is stretched between two counter-propagating laser beams using an optical stretcher. Our models, with the data, suggest that the outer actin cortex is the main determinant of the structural response of the cell.

WHILE a cell moving in the body is soft enough to squeeze through the tissue, it is also capable of withstanding high stresses such as osmotic pressure. Thus, an eukaryotic cell can respond to a large range of applied stresses, and displays a unique deformation response (structural response). How the cell achieves such a dynamic range in its structural or mechanical properties is a question that has challenged scientists from various disciplines. Elucidating the structural properties of this complex compound material requires understanding the individual contribution of the different structural components to the overall structural response of the cell.

In an eukaryotic cell, the main determinant of the structural response is the cytoskeleton – the *in vivo* polymer network that spans the interior of the cell. The cytoskeleton is composed of three polymers – actin, microtubules and intermediate filaments. The short actin filaments *in vivo* assemble into the actin cortex – a mesh-like structure just beneath the cell membrane. The rod-like microtubules are arranged in the cell in a hub-and-spoke array that extends radially outward to the actin cortex from the centrosome, which is located near the nucleus¹. Intermediate filaments are flexible coil-like polymers that form a fibrous network throughout the cell interior. Together, these polymers create a dynamic composite network that can change its architecture depending on the function and environment of the cell¹. Thus, it is not surprising that studies have shown a clear inter-relationship

between cell functioning and cell structural response². Hence, understanding the structural response of the cell gives us valuable insight into its functioning also.

Thus, the main aim of our work and this theoretical article is to model and understand the structural response of an eukaryotic cell to an applied surface stress. To create structural models for a cell, we exploit the symmetric spherical geometry of a suspended cell – a cell not attached to a substrate – and the compartmentalization of its structural elements. Our models are based on observations from the optical stretcher experiment (Figure 1), which traps individual suspended cells using two divergent counter-propagating laser beams and deforms them by a radiation-induced surface stress. Using these models, we investigate how the structural response of the cell is related to the mechanical properties of the individual cytoskeletal polymers. On building a thick shell model for the actin cortex and a three-layered model for the entire cell (with the three layers being the actin cortex, the interior polymer network and the nucleus), we use them to analyse data obtained by deforming normal NIH-3T3 and BALB-3T3 fibroblasts (fibroblasts are connective tissue cells), and malignantly transformed SV-T2 fibroblasts in the optical stretcher. For a homogeneous global stress acting on a fibroblast, we find that while the interior polymer network of the cell and the nucleus influence its exact deformed shape, it is the outer actin cortex that is the main determinant of the structural response of the cell.

Theory and modelling

Surface stress on a cell deformed in the optical stretcher

Before we consider the structural models we have created for a suspended cell, let us consider the surface stress acting on a cell in the optical stretcher. The surface stress \mathbf{s} on the cell can be calculated using ray optics and the principle of conservation of momentum. These numerical calculations, described in detail earlier^{3,4}, show that the force on the cell is outward and normal at every surface point. This global axisymmetric surface stress \mathbf{s} deforming the cell is a complicated function of the momentum transferred at the cell

*For correspondence. (e-mail: revathi@ucdavis.edu)

surface and the Gaussian intensity profile of the laser beam, and hence is analytically intractable⁴. However, due to the symmetry of the problem, we are able to find an analytic function that approximates our numerical ray optics result for \mathbf{s} to within 2%; this closed form analytic approximation to the numerically calculated \mathbf{s} is obtained for each cell stretched, and is what is used in our further structural analysis. Now, the numerically obtained \mathbf{s} on the cell can be categorized into one of three cases based on the ratio w/r , where w is the half width of the laser beam at the cell and r is the radius of the cell: (i) $w/r < 1$, (ii) $w/r \sim 1$ and (iii) $w/r > 1$. For each of these cases, an example of the analytic approximation to the numerically obtained stress \mathbf{s} is shown in Figure 2; the function is $\mathbf{s} = \mathbf{s}_0 \cos^2 \mathbf{f}$ for $w/r = 1.1$; $\mathbf{s} = \mathbf{s}_0 |\cos \mathbf{f}|^{0.5}$ for $w/r = 1.5$ and $\mathbf{s} = \mathbf{s}_0 \cos^{24} \mathbf{f}$ for $w/r < 1$, where \mathbf{f} is the polar angle and \mathbf{s}_0 is the peak stress on the cell. For $w/r < 1$, the $\cos \mathbf{f}$ exponent (i.e. $\cos^n \mathbf{f}$) depends on how small the ratio w/r is compared to 1. We have used a maximum exponent of 24 for the optical stretcher data on fibroblasts. Thus, \mathbf{s} depends sensitively on w/r . By an experimental control of this ratio, \mathbf{s} can range from a more localized stress for $w/r < 1$, mathematically described by high powers of $\cos \mathbf{f}$, to a global or

more uniform stress on the whole cell for $w/r > 1$, mathematically described by fractional powers of $\cos \mathbf{f}$.

The peak stress \mathbf{s}_0 on the cell is independent of cell size, but depends on the laser beam intensity and the relative refractive index as follows:

$$\mathbf{s}_0 = \frac{I(0)n_1}{c} (R^2(1+n) - (1-n)(R-2)), \quad (1)$$

where $I(0)$ is the maximum laser intensity, c the velocity of light, R the coefficient of reflection of light at $\mathbf{f} = 0$ and n the relative refractive index of the cell. For a constant n , the peak stress on the cell depends mainly on the laser intensity and lies in the range of 1–15 Pa for laser powers between 0.1 and 1.7 W. The normal fibroblasts show a corresponding stretching of 2–8% along the laser axis and a compression of 1–3% perpendicular to it. These small deformations enable us to perform structural analysis in the linear regime.

Modelling fibroblasts in the stretcher

Analytic thick shell elastic model for actin cortex: Ample experimental evidence, albeit more indirect and qualitative, shows that out of the three cytoskeletal polymers, actin dominates the cell's structural response^{5–8}. Hence, in our first approach to model a suspended, spherical fibroblast in the optical stretcher and quantify the individual structural role of the various cytoskeletal polymers, we assume the actin cortex to be its main structural component and neglect the other interior components. In a suspended cell, the actin cortex is a thick shell-like structure beneath the cell membrane⁹; so we model the cortex as an isotropic elastic thick shell with a hollow interior. The radial deformation of a thick shell to an axi-symmetric stress depends on the geometry of the shell and inversely on its shear modulus¹⁰. When the radial deformation of the cell and the cortex thickness are known from the experiment, as in our case, we can use this analytic result for the radial deformation of a thick shell to obtain the elasticity – shear modulus G – of the actin cortex.

To test our modelling approach, we have observed the radial extension along the laser axis (Z) and compression perpendicular to the laser axis (X) of 30 cells each of normal NIH-3T3 and BALB-3T3, and malignantly transformed SV-T2 fibroblasts in the optical stretcher. Their structural response is viscoelastic for timescales of 1 s or more, but is purely elastic when the cells are stretched for only 0.2 s. The elastic deformation data are what we model. The cortex thickness – estimated from our fluorescence images⁹ – of a suspended NIH-3T3 or BALB-3T3 fibroblast is 17–23% of the cell radius, while that of the SV-T2 fibroblast is 12–15%.

The radial deformation w of a linearly elastic shell of any thickness $h = r_0 - r_1$ (where r_0 is the outer radius and r_1 is the inner radius) due to an arbitrary axi-symmetric surface stress can be found using thick shell elasticity theory, and is given as follows¹⁰:

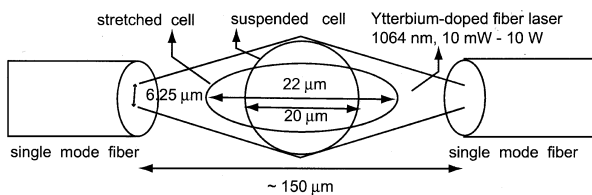


Figure 1. Schematic of a cell deforming in the optical stretcher set-up. The cell is trapped by two counter-propagating laser beams and stretched along the laser axis and compressed perpendicular to it by radiation-induced surface stress.

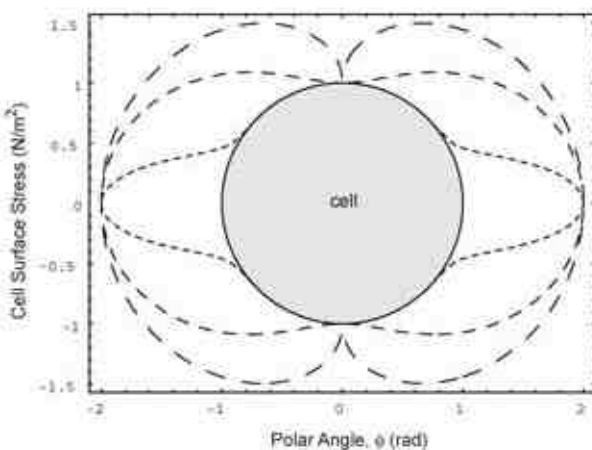


Figure 2. Polar plot of mathematical functions that approximate ray optics calculations for the surface stress \mathbf{s} on a cell in the optical stretcher, for three different ratios of half width of the laser beam at the cell (w) to the radius of the cell (r). These functions are $\mathbf{s} = \mathbf{s}_0 \cos^2 \mathbf{f}$ for $w/r = 1.1$ (medium dashes), $\mathbf{s} = \mathbf{s}_0 |\cos \mathbf{f}|^{0.5}$ for $w/r = 1.5$ (large dashes) and $\mathbf{s} = \mathbf{s}_0 \cos^{24} \mathbf{f}$ for $w/r < 1$ (small dashes), where \mathbf{f} is the polar angle. \mathbf{s}_0 , the peak stress on the cell at $\mathbf{f} = 0$, is 1 Pa here for all three cases.

$$w = \sum_n \left[A_n r^{n+1} (n+1)(n-2+4\mathbf{n}) + B_n r^{n-1} n + \frac{C_n}{r^n} n(n+3-4\mathbf{n}) - \frac{D_n(n+1)}{r^{n+2}} \right] P_n(\cos \mathbf{f}), \quad (2)$$

where r is the radial distance of any point inside the shell, ν the Poisson ratio of the material, \mathbf{f} the polar angle, P_n are Legendre polynomials of order n , and A_n, B_n, C_n, D_n are constants. At the outer radius r_0 , where the relative radial deformation w/r_0 is measured in the optical stretcher experiment, w/r_0 can be written in the form:

$$\frac{w}{r_0} = \frac{\mathbf{s}_0 F_G(r_0, \eta, \mathbf{f}, \mathbf{n})}{G}, \quad (3)$$

where \mathbf{s}_0 is the peak stress on the cell, G the shear modulus of the shell (actin cortex) and F_G the geometric factor of the thick shell, which depends on the spherical shape of the object and the applied stress distribution \mathbf{s} .

Equations (2) and (3) give the general form of shell deformation for an arbitrary axi-symmetric stress. The exact deformation to a certain stress (e.g. $\mathbf{s}_0 \cos^2 \mathbf{f}$) is obtained by evaluating boundary conditions, namely the radial stress \mathbf{s}_r (eq. (4))¹⁰ and meridional (shear) stress $\mathbf{s}_{r\mathbf{f}}$ (eq. (5))¹⁰ at both the outer surface r_0 and inner surface r_1 of the shell. In the optical stretcher, an external radial stress (e.g. $\mathbf{s} = \mathbf{s}_0 \cos^2 \mathbf{f}$) is applied at r_0 , and there is no internal radial stress at r_1 ; the applied shear stress at r_0 and r_1 is zero from our ray optics calculations. These boundary conditions yield four equations to determine A_n, B_n, C_n and D_n for every n . Note that the radial stress \mathbf{s}_r applied at r_0 is written using P_n s as the basis, and n is the order of P_n in the nonzero coefficients of the radial stress expansion (e.g. for $\mathbf{s} = \mathbf{s}_0 \cos^k \mathbf{f}$, only the terms $n = 0, 2, 4 \dots k$ are present). The shell's total radial deformation is a summation over n .

$$\frac{\mathbf{s}_r}{G} = \sum_n \left[A_n r^n (n+1)(n^2 - n - 2 - 2\mathbf{n}) + B_n r^{n-2} n(n-1) - \frac{C_n}{r^{n+1}} n(n^2 + 3n - 2\mathbf{n}) + \frac{D_n(n+1)(n+2)}{r^{n+3}} \right] P_n(\cos \mathbf{f}), \quad (4)$$

$$\frac{\mathbf{s}_{r\mathbf{f}}}{G} = \sum_n \left[A_n r^n (n^2 + 2n - 1 + 2\mathbf{n}) + B_n r^{n-2} (n-1) - \frac{C_n}{r^{n+1}} (n^2 - 2 + 2\mathbf{n}) - \frac{D_n(n+2)}{r^{n+3}} \right] \frac{dP_n(\cos \mathbf{f})}{d\mathbf{f}}. \quad (5)$$

Using the thick shell model, we obtain quantitatively meaningful values for the elasticity of the actin cortex of fibroblasts (given later in the article). Although the model accurately describes cell shape for a localized surface

stress as on the NIH-3T3 and BALB-3T3 cells, it does not satisfactorily describe the observed cell shape for a global surface stress, as on SV-T2 cells (shown later in the article). We thus create a structural model for the whole cell with a focus on the SV-T2 data.

Three-layered sphere model – Coupling between different structural elements: Experiments done in another group on deforming fibroblasts with glass needles show that these cells respond to the needles according to a three-layered model, with the three layers being the actin cortex, the interior assembly of polymers including microtubules, intermediate filaments and actin, and finally the nucleus¹¹. Thus, these results suggest that such a three-layered solid is one possible structural model for the whole cell, similar to that used for neutrophils¹². In our three-layered model cell (Figure 3), we define each homogeneous, isotropic continuum layer to have a different shear modulus G and Poisson ratio \mathbf{n} . The analytical equations used to obtain the deformation of this composite elastic sphere to an axi-symmetric stress are similar to those of the thick hollow shell. Here, each layer can be treated individually as a thick shell (the cortex and the interior network layers) or as a sphere (nucleus) (C_n s and D_n s in equations (2), (4), (5) are 0 for a sphere) with appropriate boundary conditions at the interface of the layers.

The boundary conditions used to solve the problem can be either rigid (no slip between layers) or slip boundary conditions (the surfaces can slip or move past each other) everywhere on the two interfaces. We use mixed boundary conditions (eq. (6)), a combination of no slip and slip conditions, which permit points on the two surfaces to both inter-penetrate in the radial direction and slip in the meridional direction. This non-rigid coupling between the layers (Figure 3) enables us to approximate the structural interaction between the actin cortex and the interior polymer network, and also the interaction between this polymer network and the nucleus. However, the complexity of these interactions *in vivo* makes it difficult to determine the exact boundary conditions at the actin–interior network interface and the nuclear interface. Hence, we use the three-layered model with the mixed boundary conditions and vary the \mathbf{a} s and \mathbf{b} s in them (eq. (6)) to fit our elastic experimental data and gain insight into these cytoskeletal interactions:

$$\mathbf{a}(\mathbf{s}_r)_2 = \mathbf{b}(w_2 - w_1), \quad \mathbf{a}_1(\mathbf{s}_{r\mathbf{f}})_2 = \mathbf{b}_1(v_2 - v_1), \quad (6)$$

$$(\mathbf{s}_r)_1 = (\mathbf{s}_r)_2, \quad (\mathbf{s}_{r\mathbf{f}})_1 = (\mathbf{s}_{r\mathbf{f}})_2,$$

where \mathbf{s}_r and $\mathbf{s}_{r\mathbf{f}}$ are the radial and shear stresses, w and v are the radial and meridional displacements, and 1 and 2 denote two surfaces with an interface, $\mathbf{a}, \mathbf{b}, \mathbf{a}_1$ and \mathbf{b}_1 are the interaction parameters that can be adjusted anywhere between 0 and 1 to obtain a boundary condition that varies from no-slip to slip.

Data analysis with the three-layered model yields the surprising result that the optical stretcher predominantly

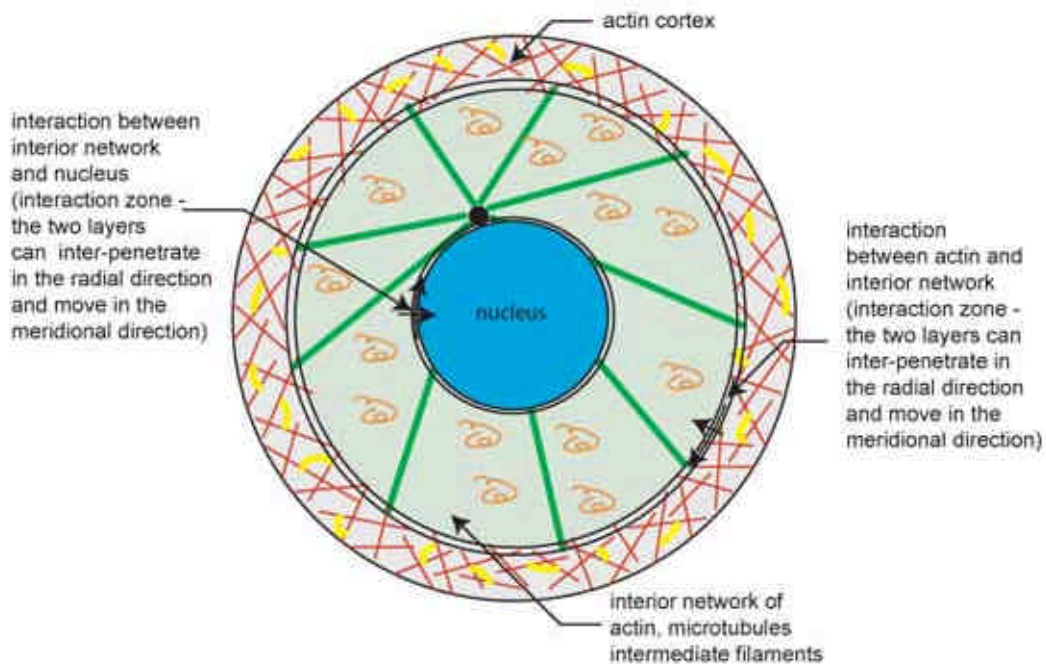


Figure 3. A possible three-layered structural model for the entire fibroblast (mainly the SV-T2 cells), consisting of actin cortex, interior polymer network of microtubules, intermediate filaments and actin, and nucleus.

deforms the actin cortex in spite of stronger structural elements in the interior, such as the microtubules and nucleus (shown later in the article). One simple explanation is that, since these elements are not rigidly coupled to the cortex in the model, their impact on the deformation of the model is seen only in the direction perpendicular to the laser axis. To further investigate the role of coupling on the structural effect of the interior network, we consider the extreme case of rigid coupling and perform a numerical finite element simulation that focuses on the microtubules and incorporates their cellular architecture and rod-like structure. Intermediate filaments are excluded since they play a role only at large deformations¹³.

Finite element simulation – Further investigation on the role of coupling: Our finite element simulation (Figure 4), created with the package ABAQUS, involves specifying the geometry of the components, the structural properties of the model's materials, such as the Young's modulus E and Poisson ratio ν , boundary conditions and applied load. In our simulation the actin cortex is an isotropic elastic shell, the microtubules are hollow elastic rods with a radius of 12 nm and a wall thickness of 5 nm and the nucleus is a solid elastic sphere. The microtubules are rigidly attached to both the nucleus and the cortex. Accuracy of the finite element code can be tested by first performing a simulation with a thick shell alone (no microtubules or nucleus) and comparing its deformation with that of the analytic thick shell model. The relative difference between the two deformations is found to be $\sim 10^{-5}$. This accuracy enables us to further in-

vestigate the microtubule–actin coupling, and the effect of the position of the nucleus on the structural response of the cell.

Results: Insights from models and experiment

Determination of actin cortex elasticity from the thick shell model

The radial deformation of a thick shell (eq. (3)) is used to obtain the shear modulus G of the actin cortex from the optical stretcher deformation data. In eq. (3), G is the only unknown quantity since the experimental cell deformation along the laser axis ($f=0$ in eq. (3)) and the cortex thickness are known, and the peak stress and stress distribution for each cell can be calculated using ray optics as discussed earlier. We then obtain, using eq. (3), G for each cell from data using a shell thickness (from fluorescence images) of 20% for the normal NIH-3T3, BALB-3T3 fibroblasts and 15% for the malignantly transformed SV-T2 fibroblasts. We then obtain the following average G for the actin cortex of each cell type: 221 ± 14 Pa for NIH-3T3, 191 ± 25 Pa for BALB-3T3 and 212 ± 15 Pa for SV-T2 fibroblasts for a Poisson ratio ν of 0.5. This is a reasonable assumption for ν since we study the initial elastic response of a transiently cross-linked polymer network. Although SV-T2 cells have a similar shear modulus to that of the NIH-3T3 and BALB-3T3 cells, their thinner actin shell gives rise to a weaker and more easily deformable structure.

Thick shell model describes deformed cell shape for a localized stress

Approximately 95% of the NIH-3T3 and 70% of the BALB-3T3 fibroblasts have been subjected to a more localized stress of $\cos^n \mathbf{f}$ with $14 \leq n \leq 24$, while $\sim 90\%$ of the SV-T2 fibroblasts have been subjected to a more global stress of $\cos^n \mathbf{f}$ with $4 \leq n \leq 14$ that deforms the whole cell. We find that the Z/X ratio, defined as the ratio of the deformation along the laser axis to that perpendicular to the laser axis, predicted by the thick shell model agrees well with the experimental Z/X ratio for all the NIH-3T3 and BALB-3T3 cells subjected to a localized stress distribution ($(Z/X_{\text{thick-shell}})/(Z/X_{\text{expt}}) \sim 1$) (Figure 5). However, the predicted Z/X ratio is much higher than that from experiment for the SV-T2

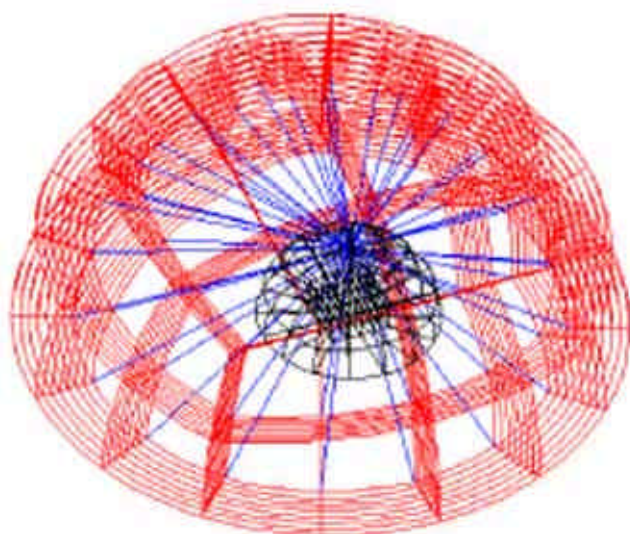


Figure 4. Finite element model for a suspended spherical cell in the stretcher: the shell-like actin cortex (red), rod-like microtubules (blue) and spherical nucleus at the centre (black). An estimate for the number of microtubules *in vivo* is ~ 1500 , but only ~ 60 microtubules are shown here for clarity. Also only a ‘half-cell model’ is required due to the symmetry of the problem.

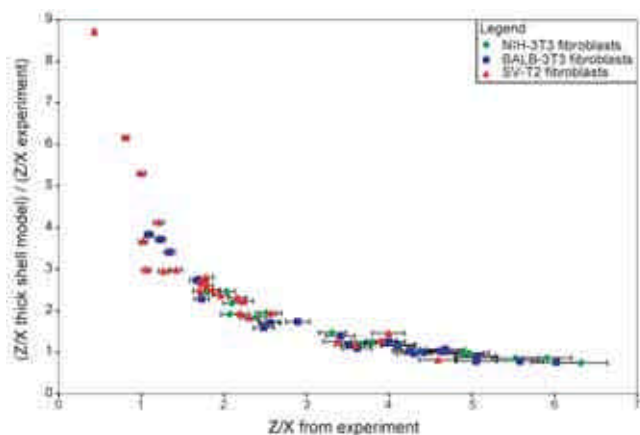


Figure 5. Comparison of Z/X ratio (defined as the ratio of cell deformation along the laser axis to that perpendicular to it) from the optical stretcher data to that predicted by thick shell theory.

cells, which have been subjected to a more global stress distribution (Figure 5).

Three-layered model – structural effect of actin–interior network coupling and role of interior elements

Using the three-layered model with the mixed boundary conditions of eq. (6) to fit the SV-T2 data, we observe that when $\mathbf{a}_i = \mathbf{b}_i = 1$, for $i = 1, 2$ in eq. (6), the Z/X ratio of the model can better explain the SV-T2 data. The mixed boundary conditions with $\mathbf{a}_i = \mathbf{b}_i = 1$, for $i = 1, 2$, imply that there is some, but not total penetration and slipping of the layers due to cytoskeletal interactions. This result is reasonable because with rigid boundary conditions at the two interfaces ($\mathbf{a}_i = 0$, $i = 1, 2$), the structure behaves like a solid sphere, whose predicted deformation is much smaller than the experimentally observed deformation (Figure 6a). On the other hand, slip conditions ($\mathbf{b}_i = 0$, $i = 1, 2$) imply that there is no coupling between the layers, while the different layers are actually connected by various crosslinking proteins. This coupling, however, is not rigid but is governed by the association and dissociation rates of these proteins with the cytoskeletal polymers.

With these mixed boundary conditions at the actin–interior network interface, the deformation of this model along the laser axis (Z) to a $\mathbf{s}_0 \cos^n \mathbf{f}$ stress is close to that of the thick shell model, while the deformation perpendicular to the laser axis (X) is affected by the interior network. This causes a decrease in the Z/X ratio from that of the thick-shell model, as seen in Figure 6a, which compares the deformation predicted by the thick shell and the three-layered model under the same stress of $10 \cos^4 \mathbf{f}$. The Z/X ratio decreases from the calculated value of 3.17 for the thick shell with $n = 0.5$ and independent of the modulus of the shell, to 2.78 for the three-layered sphere with mixed boundary conditions ($\mathbf{a}_i = \mathbf{b}_i = 1$, $i = 1, 2$), depending on the modulus and sizes of the layers. This general trend in the decrease of the Z/X ratio with the three-layered model leads to a better fit for the SV-T2 cells. As seen in Figure 6b, the predicted deformation of the three-layered model is a closer fit to the observed deformation of a representative SV-T2 fibroblast than that of the thick-shell model. While producing a fit with the three-layered model, it is hard to determine an effective value that can be used for the modulus of the interior network of microtubules, intermediate filaments and actin. So, we change this value from 100 Pa on the order of the modulus of the actin cortex, to 50,000 Pa, two magnitudes higher, on the order of the modulus of the microtubules. Since their persistence length (a measure of filament rigidity) is ~ 300 times that of actin, we assume their modulus to be two orders of magnitude higher. We find that this change in modulus causes a change in deformation of only $\sim 0.4\%$ along the laser axis, which clearly shows that the deformation of the model is insensitive to the strength of the interior network. Finally, we quantify, in Figure 6c, the difference in

the Z/X prediction of the three-layered model and that of the thick shell model ($|Z/X_{\text{three-layered}} - Z/X_{\text{thick shell}}|$) for all SV-T2, NIH-3T3 and BALB-3T3 fibroblasts. This quantitative comparison shows that the three-layered model is a consistent improvement over the thick shell model in describing the shape of all but two of the 24 SV-T2 fibroblasts analysed, but is not required for $\sim 40\%$ of the NIH-3T3 and $\sim 30\%$ of the BALB-3T3 fibroblasts. Based on the above result (Figure 6c), we calculate the modulus values for the actin cortex from the three-layered model for all the SV-T2 fibroblasts, except for the two cells that do not show an improvement with the three-layered model. We also obtain the modulus for only those NIH-3T3 and BALB-3T3 cells

whose observed shape can be explained better by the three-layered model. The modulus of the actin shell in the three-layered model has to be lowered from the 212 ± 15 Pa obtained from the thick shell model for SV-T2 cells to 186 ± 17 Pa, to fit the data.

With the three-layered model, we also analyse the effect of nuclear stiffness and size on the structural response of the cell. This study demonstrates that for the mixed boundary conditions with all \mathbf{a} , $\mathbf{b} = 1$, the change in deformation along the laser axis is $\sim 0.2\%$ due to a change in nuclear size from 3 to 6 μm in a 10 μm cell, and that due to a change in nuclear stiffness from 100 to 10,000 Pa is insignificant for $\mathbf{n} = 0.5$. However, the nucleus is important in controlling the deformation of the cell in the direction perpendicular to the laser axis and in decreasing the Z/X ratio from that of the thick shell model.

The three-layered model, thus, better explains both the deformation and cell shape of the elastic part of the optical stretcher data for the SV-T2 cells and clearly shows that the optical stretcher predominantly probes the structural strength of the actin cortex.

Finite element simulation: Further investigations of coupling, and the nucleus

The effect of microtubules: The deformation from our finite element code incorporating the cortex and microtubules is used to study whether the low structural contribution of the interior network arises from the coupling conditions alone. This was done by taking the ratio of the deformation along the laser axis from this code to that from a thick shell cortex model with no microtubules (this ratio is a measure of the contribution of microtubules to cell strength). The deformation along the laser axis in both the thick shell model and the thick shell with microtubules code is observed for the global surface stress $\mathbf{s}_0 \cos^2 \mathbf{f}$, which we use as a representative global stress for the SV-T2 cells in this study. To use the finite element code with the cortex and microtubules, we need a reasonable estimate of the number

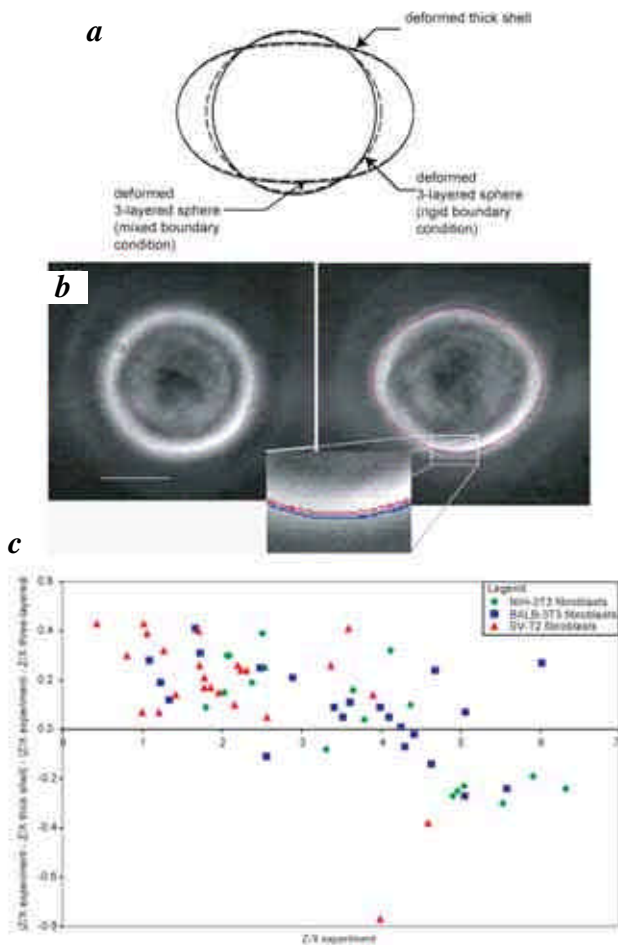


Figure 6. Analysis of fibroblasts using three-layered model. *a*, Difference in Z/X ratio of the thick shell and three-layered model under a stress $\mathbf{s}_0 \cos^2 \mathbf{f}$ for both rigid and mixed boundary conditions (deformation shown is magnified by 5). *b*, Fit of thick shell model and three-layered model to SV-T2 fibroblast. Scale bar is 10 μm . (Inset) Three-layered model (blue line) can explain the observed deformation perpendicular to the laser axis, more closely than the thick shell model (red line). We use a 15% thick shell of modulus 173 Pa, while the parameters used for the three-layered model to match its deformation along the laser axis to that of the thick shell model are: A 15% thick actin cortex of modulus 145 Pa, an interior network of shell thickness 55% and a modulus of 100 Pa, a nucleus of thickness 30% and a modulus¹⁶ of 1000 Pa. *c*, Difference in prediction of Z/X ratio of thick shell model and three-layered model for SV-T2, NIH-3T3 and BALB-3T3 fibroblasts deformed in the optical stretcher.

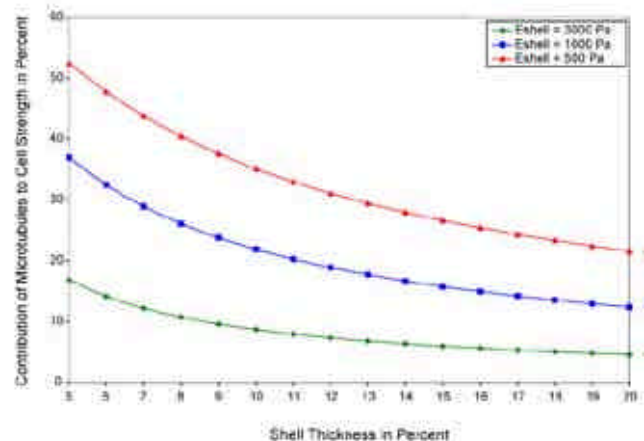


Figure 7. Parameter study to investigate the role of coupling on the structural effect of the interior network, focusing on microtubules.

of microtubules *in vivo*. This is obtained with a knowledge of the α -tubulin content, $C_{\alpha\text{-tubulin}}$, *in vivo* (e.g. $C_{\alpha\text{-tubulin}} = 1.64$ pg in neutrophils¹⁴), and the structure of a single microtubule. Each microtubule is composed of 13 protofilaments with alternating α -tubulin and β -tubulin subunits, each of ~ 50 kDa weight and 4 nm diameter. With this information, the amount of α -tubulin in a single microtubule, $C_{\text{single microtubule}}$, can be calculated if the length of the microtubule is known. We assume a microtubule length of $8\ \mu\text{m}$ for a $2\ \mu\text{m}$ thick actin cortex since the cell radius is taken to be $10\ \mu\text{m}$. Similarly, we assume corresponding microtubule lengths for other cortex thicknesses. Using $C_{\alpha\text{-tubulin}}$ in neutrophils as a representative value and a microtubule length of $8\ \mu\text{m}$, we estimate the number of microtubules *in vivo* as $C_{\alpha\text{-tubulin}}/C_{\text{single microtubule}}$, which yields a value of 1500. With this estimate, we can now use our finite element model with the cortex and microtubules to investigate the effect of microtubules on cell strength (Figure 7). In our parameter study analysing the structural contribution of the microtubules (Figure 7), we assume the microtubules to have a Young's modulus E of 50,000 Pa. Since their persistence length is ~ 300 times that of actin, we assume their E to be two orders of magnitude higher.

Using the results from the thick shell model for the cortical Young's modulus E of NIH-3T3, BALB-3T3 and SV-T2 fibroblasts ($E \sim 3G$ for $\nu = 0.5$), and their shell thickness, the contribution of microtubules to cell strength relative to the actin cortex from Figure 7 is 18.5, 20 and 23% for the NIH-3T3, BALB-3T3 and SV-T2 fibroblasts respectively. These values can vary due to the dispersity in the Young's modulus of microtubules reported in the literature¹⁵. Also, the above values overestimate the contribution from the microtubules since we consider rigid coupling between the microtubules and the actin cortex. In general, our results demonstrate that as the thickness and modulus of the actin shell increase, contribution from the microtubules to cell strength diminishes exponentially. This suggests that even in the case of rigid coupling of the rods to the cortex, it is the outer shell that is the main determinant of the structural response of the cell. Hence, we conclude that coupling alone is not responsible for the subordinate structural role of the cell interior.

Structural impact of asymmetry in the position of the cell nucleus: The nucleus of the cell is an approximately spherical object of Young's modulus¹⁶ ~ 1000 Pa. Our fibroblast images show that the nucleus is not situated at the centre of the cell, but is displaced $1\text{--}2\ \mu\text{m}$ from the centre in any direction. Our finite element simulation of the cell (Figure 4) allows us to place the nucleus anywhere in the XY plane, a feature that cannot be easily incorporated in our analytical three-layered model. In a $10\ \mu\text{m}$ cell, when the nucleus is displaced $1\text{--}2\ \mu\text{m}$, the deformation at the cell surface does not change measurably. This suggests that the effect of the asymmetry of the nucleus on the structural response of the cell is not significant.

Summary

We have created two structural models for a suspended cell being deformed in the optical stretcher. Although a thick shell cortex model accurately explains the observed cell shape for a localized stress on the cell (NIH-3T3 and BALB-3T3 cells), a three-layered model that considers the interior structural elements is required to explain cell shape for a global surface stress (SV-T2 cells). The three-layered model along with our finite element simulations reveals that the cell deformation is insensitive to the strength of the interior network or nucleus. Although these interior elements influence the exact shape of the deformed cell, it is the outer actin shell that mainly determines the structural response of the cell.

1. Lodish, H., Berk, A., Zipursky, L. S., Matsudaira, P., Baltimore, D. and Darnell, J., *Molecular Biology of the Cell*, W. H. Freeman and Company, New York, 2000, 4th edn.
2. Malek, A. M. and Izumo, S., Mechanism of endothelial cell shape change and cytoskeletal remodeling in response to fluid shear stress. *J. Cell Sci.*, 1996, **109**, 713–726.
3. Guck, J., Ananthakrishnan, R., Moon, T. J., Cunningham, C. C. and Kas, J., Optical deformability of soft biological dielectrics. *Phys. Rev. Lett.*, 2000, **84**, 5451–5454.
4. Guck, J., Ananthakrishnan, R., Mahmood, H., Moon, T. J., Cunningham, C. C. and Kas, J., The optical stretcher: A novel laser tool to micromanipulate cells. *Biophys. J.*, 2002, **81**, 767–784.
5. Elson, E. L., Cellular mechanics as an indicator of cytoskeletal structure and function. *Annu. Rev. Biophys. Biophys. Chem.*, 1988, **17**, 397–430.
6. Stossel, T. P., Contribution of actin to the structure of the cytoplasmic matrix. *J. Cell Biol.*, 1984, **99**, 15s–21s.
7. Sato, M., Theret, D. P., Wheeler, L. T., Ohshima, N. and Nerem, R. M., The application of a homogeneous half-space model in the analysis of endothelial cell micropipette measurements. *J. Biomech. Eng.*, 1990, **112**, 263–326.
8. Rotsch, C. and Radmacher, M., Drug induced changes of cytoskeletal structure and mechanics in fibroblasts: An atomic force microscopy study. *Biophys. J.*, 2000, **78**, 520–535.
9. Guck, J. *et al.*, Optical deformability as an inherent cell marker for testing malignant transformation and metastatic competence. *Biophys. J.*, 2005, **88**, 3689–3698.
10. L'ure, A. I., *Three Dimensional Problems of the Theory of Elasticity*, Interscience Publishers, New York, 1964.
11. Heidemann, S. R., Kaech, S., Buxbaum, R. E. and Matus, A., Direct observations of the mechanical behaviors of the cytoskeleton in living fibroblasts. *J. Cell Biol.*, 1999, **145**, 109–122.
12. Tran-Son-Tay, R., Kan, H. C., Udaykumar, H. S., Damay, E. and Shyy, W., Rheological modelling of leukocytes. *Med. Biol. Eng. Comput.*, 1998, **36**, 246–250.
13. Wang, N. and Stamenovic, D., Contribution of intermediate filaments to cell stiffness, stiffening, and growth. *Am. J. Physiol., Cell Physiol.*, 2000, **279**, C188–C94.
14. Olins, A. L., Herrmann, H., Lichter, P. and Olins, D. E., Retinoic acid differentiation of HL-60 cells promotes cytoskeletal polarization. *Exp. Cell Res.*, 2000, **254**, 130–142.
15. Kis, A. *et al.*, Nanomechanics of microtubules. *Phys. Rev. Lett.*, 2002, **89**, 248101–248104.
16. Guilak, F., Tedrow, J. R. and Burgkart, R., Viscoelastic properties of the cell nucleus. *Biochem. Biophys. Res. Commun.*, 2000, **269**, 781–786.

Received 2 November 2004; revised accepted 3 March 2005